Evaluation and Improvement of a TKE-Based Eddy-Diffusivity Mass-Flux (EDMF) Planetary Boundary Layer Scheme in Hurricane Conditions

XIAOMIN CHEN,[a,b] GEORGE H. BRYAN,[c] ANDREW HAZELTON,[a,d] FRANK D. MARKS,[a] AND PAT FITZPATRICK[e]

[a] *NOAA/OAR/Atlantic Oceanographic and Meteorological Laboratory, Miami, Florida*
[b] *Northern Gulf Institute, Mississippi State University, Stennis Space Center, Mississippi*
[c] *National Center for Atmospheric Research, Boulder, Colorado*
[d] *Cooperative Institute for Marine and Atmospheric Studies, University of Miami, Miami, Florida*
[e] *Department of Physical and Environmental Sciences, Texas A&M University–Corpus Christi, Corpus Christi, Texas*

(Manuscript received 15 October 2021, in final form 17 March 2022)

ABSTRACT: Accurately representing boundary layer turbulent processes in numerical models is critical to improve tropical cyclone forecasts. A new turbulence kinetic energy (TKE)-based moist eddy-diffusivity mass-flux (EDMF-TKE) planetary boundary layer scheme has been implemented in NOAA's Hurricane Analysis and Forecast System (HAFS). This study evaluates EDMF-TKE in hurricane conditions based on a recently developed framework using large-eddy simulation (LES). Single-column modeling tests indicate that EDMF-TKE produces much greater TKE values below 500-m height than LES benchmark runs in different high-wind conditions. To improve these results, two parameters in the TKE scheme were modified to ensure a match between the PBL and surface-layer parameterizations. Additional improvements were made by reducing the maximum allowable mixing length to 40 m based on LES and observations, by adopting a different definition of boundary layer height, and by reducing nonlocal mass fluxes in high-wind conditions. With these modifications, the profiles of TKE, eddy viscosity, and winds compare much better with LES results. Three-dimensional idealized simulations and an ensemble of HAFS forecasts of Hurricane Michael (2018) consistently show that the modified EDMF-TKE tends to produce a stronger vortex with a smaller radius of maximum wind than the original EDMF-TKE, while the radius of gale-force wind is unaffected. The modified EDMF-TKE code produces smaller eddy viscosity within the boundary layer compared to the original code, which contributes to stronger inflow, especially within the annulus of 1–3 times the radius of maximum wind. The modified EDMF-TKE shows promise to improve forecast skill of rapid intensification in sheared environments.

KEYWORDS: Boundary layer; Hurricanes/typhoons; Large eddy simulations; Numerical analysis/modeling; Single column models; Subgrid-scale processes

1. Introduction

Parameterizations of boundary layer turbulent processes play an important role in governing the evolution of tropical cyclone (TC) structure and intensity (e.g., Braun and Tao 2000; Hill and Lackmann 2009; Nolan et al. 2009a,b; Smith and Thomsen 2010; Bryan 2012; Zhang et al. 2015; Bu et al. 2017; Zhang and Pu 2017; Chen et al. 2021b). Continuous development of planetary boundary layer (PBL) schemes, especially for high-wind, nearly neutral TC boundary layers, is critical to further improving forecasts of TC structure and intensity, as well as the global impact of TCs.

NOAA's Hurricane Analysis and Forecast System (HAFS; e.g., Hazelton et al. 2021) is a hurricane application of the cubed-sphere finite-volume dynamical core (FV3)-based Unified Forecast System (UFS). One of the model physics upgrades in HAFS is replacing the hybrid eddy-diffusivity mass-flux (EDMF) PBL scheme with a scale-aware turbulence kinetic energy (TKE)-based moist EDMF PBL scheme (EDMF-TKE hereafter; Han and Bretherton 2019). Recently, the shear impact on vertical mixing (Rodier et al. 2017) was included in EDMF-TKE.

In the EDMF-TKE PBL scheme, the downgradient transport is parameterized by a TKE-based eddy-diffusivity approach; the counter-gradient transport by large eddies is parameterized by a mass-flux approach that is applicable to all unstable boundary layer conditions. Additionally, parameterizations of mixing length and dissipation length scale in EDMF-TKE follow Bougeault and Lacarrere (1989), and their study showed that these length scales work well in low-wind, convective boundary layers. Given that the EDMF-TKE scheme is not specifically designed for high-wind conditions like hurricanes, this study is motivated to evaluate this new scheme in hurricane conditions, using an evaluation framework tailored to the hurricane boundary layer proposed by Chen et al. (2021a). It is worth noting that the parameterized mass fluxes in EDMF-TKE are scale-aware to horizontal grid spacings (Δ), i.e., mass fluxes decrease with decreasing horizontal grid spacings if $0.1 < \Delta/h < 1$ (i.e., the model gray zone, Arakawa et al. 2011), where h is boundary layer depth. In this study, we focus on mesoscale grid spacings comparable to those used in HAFS, which are beyond gray-zone resolutions ($\Delta > h$). For the effect of scale-awareness on TC simulations, we refer interested readers to Chen et al. (2021b).

2. Methods and model setup

a. An evaluation framework for PBL schemes in high-wind conditions

In this study, we evaluate the EDMF-TKE scheme that is targeted for version 17 of the Global Forecast System

Corresponding author: Xiaomin Chen, xiaomin.chen@noaa.gov

DOI: 10.1175/WAF-D-21-0168.1

(GFS)[1] by using a numerical modeling framework tailored to the hurricane boundary layer (Chen et al. 2021a). In short, this framework allows for either a small-domain [$O(5)$ km] large-eddy simulation (LES) or a single-column modeling (SCM) simulation using the EDMF-TKE PBL scheme under the same controlled thermodynamic conditions. For LES, there are 528 × 528 grid points horizontally, and the horizontal grid spacing is 10 m. We use 500 vertical levels, with the model top of 3 km. The vertical grid spacing is 5 m below 2 km and increases to 15 m between 2 and 3 km. For SCM simulations, a very similar model setup is used except that there is only one single column and the vertical grid spacing is 20 m below 2 km. As in Chen et al. (2021a), domain-averaged turbulence properties from the LES are treated as the benchmark to evaluate the SCM simulations with the EDMF-TKE scheme. The controlled vertical profiles of thermodynamic variables come from dropsonde composites of category-4–5 hurricanes from 1999 to 2010. Using vertical profiles of thermodynamic variables outside the eyewall where the 10-m tangential wind is roughly 25 m s^{-1} (V25, hereafter), 35 m s^{-1} (V35, hereafter), and 45 m s^{-1} (V45, hereafter), respectively, three sets of experiments are performed. We use version 20 of Cloud Model 1 (CM1; Bryan and Fritsch 2002) for both LES and SCM simulations. The LES domain or SCM grid point is located due east to the TC center, and hereafter u and v denote radial and tangential winds, respectively. For more details of this framework and the related model setup, we refer interested readers to Chen et al. (2021a).

b. Model setup for idealized 3D simulations

We also use the CM1 model for idealized three-dimensional simulations. Following Chen and Bryan (2021), the model is initialized with an axisymmetric TC vortex in a quiescent environment on an f plane with a Coriolis parameter of 5×10^{-5} s^{-1}. The radial profile of the tangential wind of the initial vortex follows a modified Rankine vortex:

$$V(r) = \begin{cases} V_m \dfrac{r}{r_m}, & r \le r_m \\ V_m \dfrac{r}{r_m} \exp\left\{\dfrac{1}{B}\left[1 - \left(\dfrac{r}{r_m}\right)^B\right]\right\} - \dfrac{r - r_m}{r_0 - r_m} \exp\left\{\dfrac{1}{B}\left[1 - \left(\dfrac{r_0}{r_m}\right)^B\right]\right\}, & r > r_m \end{cases}, \tag{1}$$

where the radius of the maximum wind r_m is set to 80 km, the maximum tangential wind V_m = 20 m s^{-1} near the surface and decreases linearly to zero from the surface to 12-km height (i.e., vortex depth is 12 km), and the parameter B controlling the decay rate of tangential wind outside the r_m is set to 1.0. The term r_0 is the radius where tangential winds vanish (=500 km). The CM1 model uses one large model domain that follows the motion of simulated TCs. The horizontal grid spacing is set to 3 km within the central 600 km × 600 km area, beyond which the horizontal grid spacing is gradually stretched from 3 to 15 km in the outer portion of the domain. In the vertical direction there are 59 model levels, which are stretched in the vertical so that there are 10 model levels below 1.5-km height. The output frequency is every 1 h. The selected model physics schemes are identical with Chen and Bryan (2021), except for the PBL scheme. We perform two experiments, one using the original and a second using the modified EDMF-TKE based on LES results.

To test the robustness of results based on the comparisons of two experiments, we performed other pairs of sensitivity experiments using the original and modified EDMF-TKE by varying V_m, decay rate of the tangential wind outside the RMW, and sea surface temperature. The findings in these sensitivity experiments are consistent with the findings from the above two simulations (not shown), and we focus only on the analyses of these two simulations in section 4b.

c. Model setup for HAFS forecasts of Hurricane Michael (2018)

To examine the effect of the modified EDMF-TKE on real hurricanes, we also perform two sets of 5-member ensemble HAFS forecasts of Hurricane Michael (2018) using the original and modified EDMF-TKE schemes. Hurricane Michael rapidly intensified while over the eastern Gulf of Mexico into a category-5 hurricane at landfall. It defied some forecasts which projected steady state or even some weakening under moderate vertical wind shear (Beven et al. 2019). Hazelton et al. (2020) studied the rapid intensification of Michael using an ensemble of a high-resolution nested-FV3 model (similar to HAFS) simulations, initialized at 1800 UTC 7 October 2018, when Michael was over the northwestern Caribbean Sea and approximately 3 days before it made landfall. In this study, the 5 ensemble members in each set were initialized at −12, −6, 0, +6, and +12 h relative to 1800 UTC 7 October 2018, respectively. The 2021 baseline version of the stand-alone-regional HAFS (HAFS-SAR, Dong et al. 2020) is used. HAFS-SAR features a large static nest over the North Atlantic, Gulf of Mexico, Caribbean Sea, and eastern United States, with a horizontal grid spacing of ~3 km. The version of HAFS-SAR analyzed here uses 91 vertical levels. The references above describe some of the key model physics. This version of HAFS-SAR is coupled to the Hybrid Coordinate Ocean Model (HYCOM; Bleck 2002).

Hereafter, we refer to the SCM and idealized 3D simulations as well as HAFS forecasts using the original EDMF-TKE as the CTL experiments, and those simulations or forecasts using the revised EDMF-TKE scheme as the REV

[1] This code was provided by Drs. Jongil Han and Chunxi Zhang at NOAA/EMC.

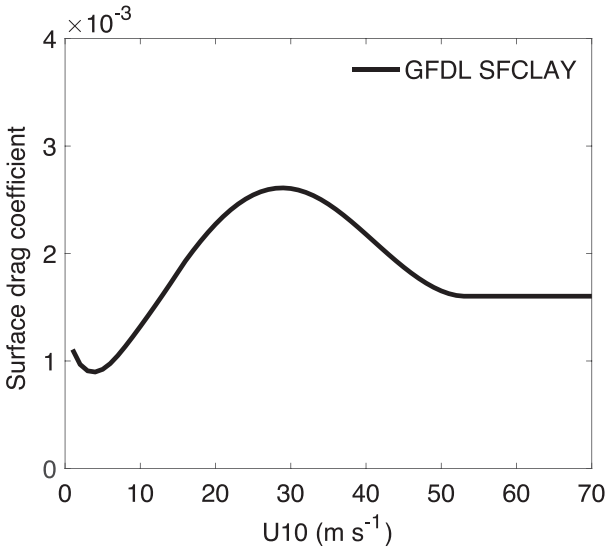

FIG. 1. The surface drag coefficient under neutral conditions as a function of 10-m surface wind in the GFDL surface-layer scheme. Adapted from Fig. 4a in Chen et al. (2021a).

experiments. The revisions to the original EDMF-TKE scheme are detailed in the next section. Of note, all of the experiments in this study use the same GFDL surface-layer scheme and the formulation of surface drag coefficient as a function of 10-m wind is shown in Fig. 1.

3. Improvement of EDMF-TKE

EDMF-TKE is a TKE-based (i.e., 1.5-order) turbulence scheme, and it is important to understand whether EDMF-TKE can produce an accurate vertical profile of TKE in hurricane conditions. Figure 2a shows TKE profiles from a SCM test using the original EDMF-TKE PBL scheme (i.e., CTL) and a LES benchmark run for V35. TKE from LES is defined as $(1/2)(\overline{u'u'} + \overline{v'v'} + \overline{w'w'}) + e_s$, where u, v, and w are the three components of velocity; overbars denote a domain average at a specified height; primes denote perturbations from the domain average; and e_s is subgrid TKE which comes from the subgrid model (see appendix of Bryan et al. 2017 for details). The TKE from CTL is much greater than the LES results below 500 m height; near the surface, the TKE from CTL is approximately a factor of 2 larger than the LES results (Fig. 2a). This finding suggests a mismatch of TKE shear production and dissipation terms in the original EDMF-TKE, which are the two largest terms in the TKE budget in hurricane conditions (e.g., Chen and Bryan 2021).

a. Matching PBL and surface-layer formulations

To improve the vertical profile of TKE, a closer examination of the TKE budget equation near the surface is performed in this section. Furthermore, we note that the proper matching of a PBL code with a surface-layer code is essential for providing expected results near the surface (Kepert 2012), where the surface layer is defined approximately as the lowest 10% of the boundary layer. Given that hurricane boundary layers, especially the lower portion, are essentially neutrally stratified in high wind speeds despite the existence of substantial surface heat fluxes (e.g., Kepert 2012; Foster 2013; Chen et al. 2021a), we assume neutral boundary layer conditions in the following derivations.

We begin by deriving a relation for diffusivity (K_m) from the PBL code, which we will later match with an analytical formulation for K_m in the surface layer. Definitions of most

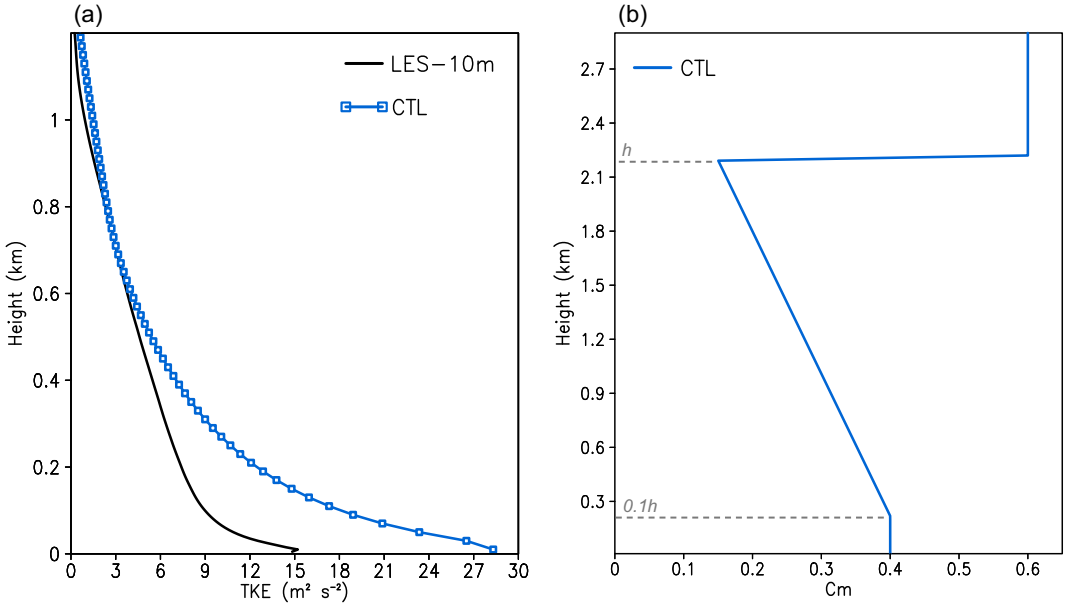

FIG. 2. (a) Vertical profile of TKE ($m^2 s^{-2}$) from LES (black) and CTL (blue) for V35. (b) Vertical profile of c_m from the CTL (blue) experiment for V35. The levels of $0.1h$ and h are marked by gray dashed lines in (b).

symbols in this section can be found in the appendix. Starting with the TKE equation, (A3), we assume the time tendency of TKE (e) and the vertical transport term are negligible {i.e., $\partial\overline{e}/\partial t = \partial\left[\overline{w'\overline{e}} + (1/\rho)\overline{w'p'}\right]/\partial z = 0$}. Because the buoyancy term is zero in neutral conditions, then the TKE budget Eq. (A3) becomes

$$-\left(\overline{u'w'}\frac{\partial\overline{u}}{\partial z} + \overline{v'w'}\frac{\partial\overline{v}}{\partial z}\right) = D, \tag{2}$$

where D is the dissipation rate. For the turbulent flux terms, we use

$$\overline{w'\phi'} = -K_\phi\frac{\partial\overline{\phi}}{\partial z}, \tag{3}$$

where K_ϕ is eddy diffusivity; note that (3) is (A1) but without the mass-flux components (which are assumed to be negligible in neutral conditions). Using the relationship (A2) between K_m (the eddy diffusivity for momentum) and e, then the formulation for D [see (A5)] can be written in terms of K_m:

$$D = \frac{C_d}{l_d}\left(\frac{K_m}{C_m l_k}\right)^3, \tag{4}$$

where l_d and l_k are length scales, C_m is a coefficient for relating K_m and e, and C_d is a coefficient for relating D and e (see the appendix for further details).[2] Using (3) and (4), then (2) can be reorganized as

$$K_m = \left[\frac{C_m^3 l_k^3 l_d}{C_d}\left(\frac{\partial\overline{u}}{\partial z}\frac{\partial\overline{u}}{\partial z} + \frac{\partial\overline{v}}{\partial z}\frac{\partial\overline{v}}{\partial z}\right)\right]^{1/2}. \tag{5}$$

Now we define $S^2 = (\partial\overline{u}/\partial z)(\partial\overline{u}/\partial z) + (\partial\overline{v}/\partial z)(\partial\overline{v}/\partial z)$, and use the same length scales for (A2) and (A5) (i.e., we assume $l_d = l_k$), which produces a general relation for eddy diffusivity from a TKE PBL scheme in neutral conditions:

$$K_m = \left(\frac{C_m^3}{C_d}\right)^{1/2} {l_k}^2 S. \tag{6}$$

The next step is to match (6) to conditions in the surface layer. Monin–Obukhov similarity theory is used for the surface layer in NWP models. For neutral stratification, the nondimensional wind shear ϕ_m in similarity theory:

$$\phi_m = \frac{\kappa z}{u_*}\frac{\partial U}{\partial z}, \tag{7}$$

simply has a value of 1. In (7), $U(z)$ is the horizontal wind speed, u_* is the surface friction velocity, and κ is the von Kármán constant. Assuming the change in wind direction is small in the surface layer, then

$$S = \frac{\partial U}{\partial z} = \frac{u_*}{\kappa z}. \tag{8}$$

[2] In this study, C_d does not denote a surface drag coefficient; instead, it is a coefficient used in the TKE dissipation term following Han and Bretherton (2019).

Now by using the momentum-flux parameterization (3) with the left-hand side set equal to the surface condition, $\overline{w'u'}|_{z=0} = -u_*^2$, and using (8) for the shear term on the right-hand side, then solving for K_m, we arrive at general relation for diffusivity in a neutral surface layer:

$$K_m = \kappa u_* z, \tag{9}$$

which is identical to Eq. (2) of Kepert (2012).

An important property of the turbulent surface layer that will prove useful is the linearity of mixing-length scale l with height:

$$l = \kappa z. \tag{10}$$

This is the well-documented "mixing length" hypothesis of Prandtl (1925), as also noted by Kepert (2012). We note that the length scale in the EDMF-TKE scheme, (A6), is equivalent to (10) for neutral conditions near the surface.

We now match the analytic result for diffusivity in a surface layer, (9), with the formulation for EDMF-TKE, (6):

$$\left(\frac{C_m^3}{C_d}\right)^{1/2} l_k^2 S = \kappa u_* z. \tag{11}$$

Using (10) for l_k and (8) for S, (11) reduces to

$$\left(\frac{C_m^3}{C_d}\right)^{1/2} = 1. \tag{12}$$

From (12), a necessary relationship between C_d and C_m in neutral surface-layer conditions is thus

$$C_d = C_m^3. \tag{13}$$

Han and Bretherton (2019) used $C_d = 0.7$ and $C_m = 0.4$, which is not consistent with (13), suggesting a mismatch between PBL and surface-layer parameterizations. In the original EDMF-TKE code we use for this study, $C_d = 0.4$, and C_m is 0.4 in the surface layer and then decreases linearly with height to the diagnosed boundary layer height (Fig. 2b); these values in the surface layer are also inconsistent with (13).

The next task is to determine a value of either C_m or C_d near the surface that either matches theory or observations, and then use (13) to determine the other parameter. To this end, we note that observations (e.g., Grant 1992), in addition to our LES results (not shown), as well as other studies of neutral boundary layers (Nieuwstadt 1984; Berg et al. 2020) find that the Reynolds shear stress normalized by TKE $u_*^2/\overline{e} \approx 0.24$ in the surface layer. Assuming again that TKE production and dissipation terms are balanced, (2) can be reorganized [using (A5), (8), and $\overline{w'u'}|_{z=0} = -u_*^2$] as

$$\frac{u_*^3}{\kappa z} = C_d\frac{\overline{e}^{3/2}}{l_d}. \tag{14}$$

Solving for C_d, and using (10) and again assuming that $l_d = l_k$, we find a relation for C_d in the neutral surface layer:

$$C_d = \left(\frac{u_*^2}{\overline{e}}\right)^{3/2}. \tag{15}$$

Following the studies cited above, we assume $u_*^2/\overline{e} \approx 0.24$ and thus, from (15), $C_d \approx 0.12$. With (13) it follows that $C_m \approx 0.5$. After performing a set of SCM tests, we set $C_m = 0.55$ and $C_d = 0.12$ in the modified EDMF-TKE. To keep the Prandtl number consistent, we accordingly set the stability coefficient for heat $C_h = 0.55$ in the surface layer. Of note, while these changes are based on the assumption of neutrality, effects of surface-layer stability from other types of boundary layers are included in the code using the Monin–Obukhov similarity theory. These changes are applied to the entire model domain of CM1 and HAFS simulations.

b. Other changes to EDMF-TKE

Another modification to the EDMF-TKE code that improves results in this study is the definition of boundary layer height, h. For context, we note that h in K-profile parameterization (KPP) PBL schemes has a profound effect on eddy viscosity (e.g., Kepert 2012), whereas h in TKE-based PBL schemes is fundamentally a *diagnostic* term that is not necessarily needed to determine K. The EDMF-TKE scheme is somewhat between the two extremes, in that the value of h has a modest effect on the vertical mixing. In EDMF-TKE, h affects the entrainment rate in the prognostic equation for updraft velocity w_u [related to surface-based mass-flux M_u, see (14) in Han and Bretherton (2019)] as well as vertical profiles of c_m and thus the TKE and K_m (see discussions in section 3a). Figure 2b indicates that the diagnosed h is ~2.2 km for CTL, which is more than 2 times the inflow layer depth for V35 (~1 km, see discussions in section 4a). Of note, observational composites of hurricanes (Zhang et al. 2011) indicates a similar inflow layer depth as in V35. The overestimation of h in CTL is found attributable to shear below the bottom model level in hurricane conditions [see definition of h_{Ric} in (A9)]. To address this overestimation, we adopted a different PBL height definition that works well in all stability conditions, including high-wind conditions (Vogelezang and Holtslag 1996), and PBL height is the level where bulk Richardson number Rib = 0.25. The definition of Rib is

$$\mathrm{Rib} = \frac{\dfrac{g}{\theta_{vs}}(\theta_{vh} - \theta'_{vs})(h - z_s)}{(u_h - u_s)^2 + (v_h - v_s)^2 + 100u_*^2}, \tag{16}$$

where z_s is the height of the bottom model level, and u_s and v_s denote meridional and zonal winds at $z = z_s$, respectively. For stable and neutral boundary layers, $\theta'_{vs} = \theta_{vs}$, where θ_{vs} is the virtual potential temperature at $z = z_s$; for unstable conditions, $\theta'_{vs} = \theta_{vs} + b\left[(w'\theta'_v)_0/w_s\right]$ (Troen and Mahrt 1986), where b is a coefficient, $(w'\theta'_v)_0$ is the virtual heat flux at the surface, and w_s is a turbulent velocity scale. The term $b\left[(w'\theta'_v)_0/w_s\right]$ is a measure of convective thermals, and it becomes important when the buoyancy production of TKE dominates over shear production. The bulk Richardson number is calculated in the layer from the bottom model level, rather than from the ground surface as in (A9). We notice that the diagnosed h is substantially reduced using the modified PBL definition (see later discussions in section 4a).

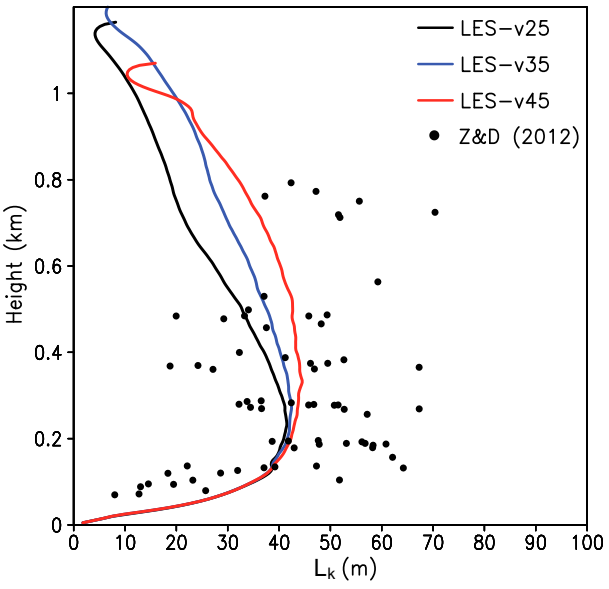

FIG. 3. Vertical profiles of mixing length from LES output averaged over t = 4–6 h. Black, blue, and red lines denote the results for V25, V35, and V45, respectively. Black dots denote in situ aircraft observations from Zhang and Drennan (2012). The LES results are from Chen et al. (2021a).

The mass-flux part of EDMF parameterizes the nonlocal turbulent transport by thermal plumes in low-wind and unstable boundary layer conditions (Siebesma et al. 2007). In EDMF-TKE, the triggering criteria for the surface-driven mass flux [i.e., the second term on the right-hand side of (A1)] is $\zeta = z_s/L < -0.02$, where L is Monin–Obukhov length. In hurricane boundary layers, strong vertical wind shear within the boundary layer can distort and tear apart the rising thermal plumes, causing a nonnegligible reduction in mass fluxes. Given this, we curtail mass fluxes based on 10-m wind speed magnitudes—mass fluxes are linearly tapered when $V_{10} \geq 20$ m s^{-1} and turned off when $V_{10} \geq 30$ m s^{-1}, following the MYNN code from version 4.2 of WRF. Note that this change is applicable to other high-wind boundary layers too.

Another important revision to the EDMF-TKE PBL scheme for hurricane conditions is the maximum allowable value of mixing length. Above the surface layer in the original EDMF-TKE, l_{BL} is capped at 300 m. However, the LESs from Chen et al. (2021a) and mean values of observations from Zhang and Drennan (2012) indicate that in hurricane conditions the maximum value of mixing length above the surface layer is ~40 m (Fig. 3). The effective mixing length from both LESs and observations is calculated as

$$l_k = (K_{\mathrm{eff}}/S)^{1/2}, \tag{17}$$

where K_{eff} is the effective eddy diffusivity in neutral conditions [see Eq. (2) in Chen et al. 2021a]. Following the results from LESs and observations, we cap l_{BL} at 40 m in the modified EDMF-TKE. As discussed earlier, the assumption of neutrality holds well in the lower to mid-hurricane boundary

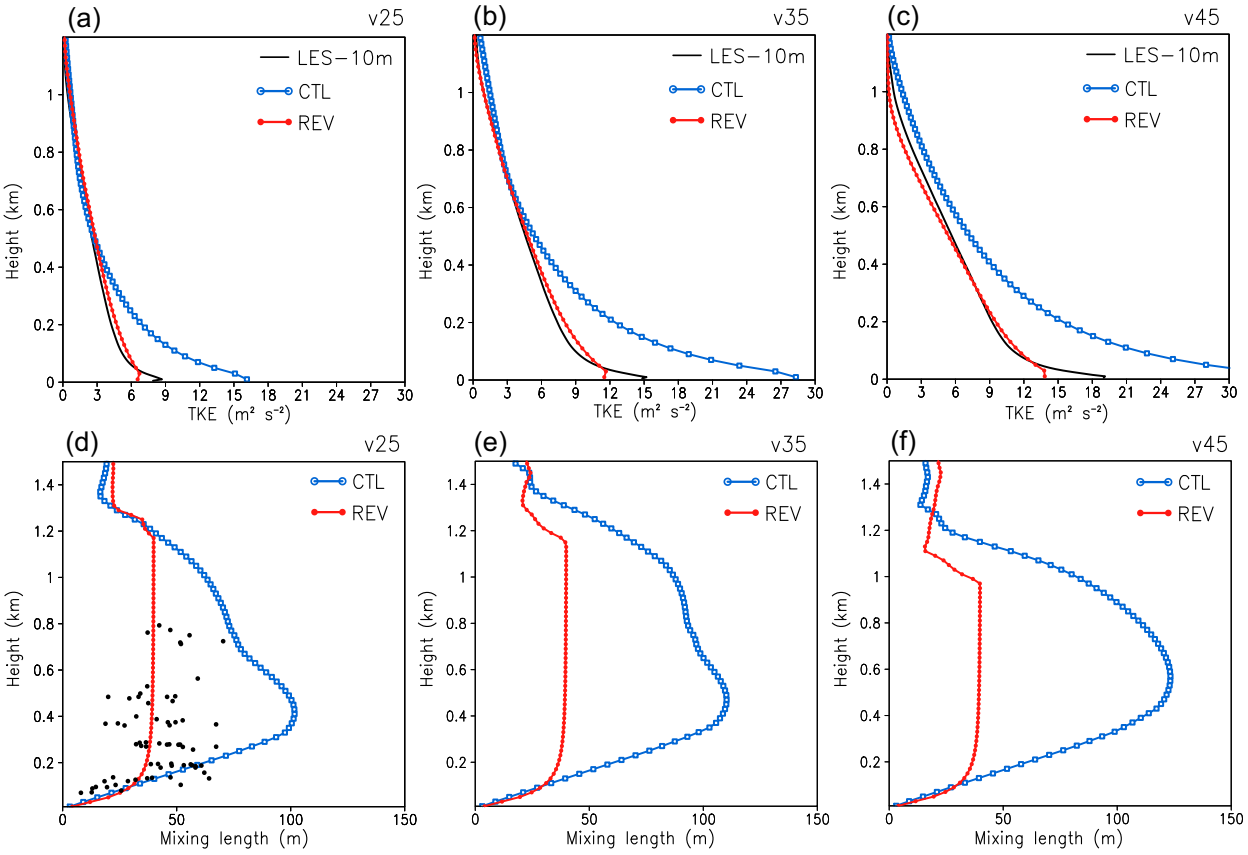

FIG. 4. (a)–(c) Vertical profile of TKE ($m^2\ s^{-2}$) from LES (black), CTL (blue), and REV (red) for V25, V35, and V45, respectively. (d)–(f) As in (a)–(c), but for mixing length (m). Black dots in (d) represent observations from Zhang and Drennan (2012).

layer. In the mid- to upper hurricane boundary layer, however, vertical wind shear is substantially smaller and buoyancy production of TKE starts to play a role; thus, cautions are needed to interpret the mixing length from both LESs and observations in that region. In this study, we apply the maximum allowable mixing length of 40 m to the entire domain of CM1 and the regional domain of HAFS-SAR. As moving-nest capabilities in HAFS become feasible in the 2022 hurricane season, we plan to apply this change solely to the moving nest or hurricane environments and retain the original maximum allowable mixing length of 300 m in the outer domain of HAFS for the consideration of daytime convective boundary layers over land. Nevertheless, we will reassess these four changes of the EDMF-TKE scheme in other types of boundary layers in future work.

4. Evaluation of the modified EDMF-TKE scheme

a. Single-column model tests

In this section, we conduct three sets of SCM tests (i.e., V25, V35, and V45, indicating the approximate values of 10-m wind speed) using the original (CTL) and modified EDMF-TKE (REV) schemes and compare the SCM results against LES benchmark runs. Consistent with Fig. 2a for V35, the CTL experiments using the original EDMF-TKE show a much larger TKE below 500 m than LES in other high-wind conditions (Figs. 4a–c). In contrast, the REV experiments using the modified EDMF-TKE exhibit a much-improved TKE profile, and differences in the magnitude of TKE between REV and LES are $<1\ m^2\ s^{-2}$ above $z = 50$ m and ~3–4 $m^2\ s^{-2}$ below $z = 50$ m. The slightly larger error in the near-surface layer (below 50 m) is partly attributable to relatively coarse vertical grid spacings used in SCM tests than in LES, which may cause an underestimation of vertical wind shear near the surface and thereby the shear production of TKE. Figures 4d–f compare the vertical profile of mixing length l_k from the CTL and REV experiments. The maximum value of l_k above the surface layer in the REV experiments is capped at 40 m, as discussed in section 4, which is more than a factor of 2 smaller than the maximum l_k in CTL. For a reference, Fig. 4d also shows available observations (see black dots) at a similar high-wind condition (Zhang and Drennan 2012). For V25, l_k from REV agrees well with these observation data below 800 m height, while l_k from CTL exceeds the maximum value of observations by approximately a factor of 2 in the 200–800-m layer.

With smaller TKE and l_k profiles in REV, it is not surprising to see that REV produces smaller K_m than CTL in

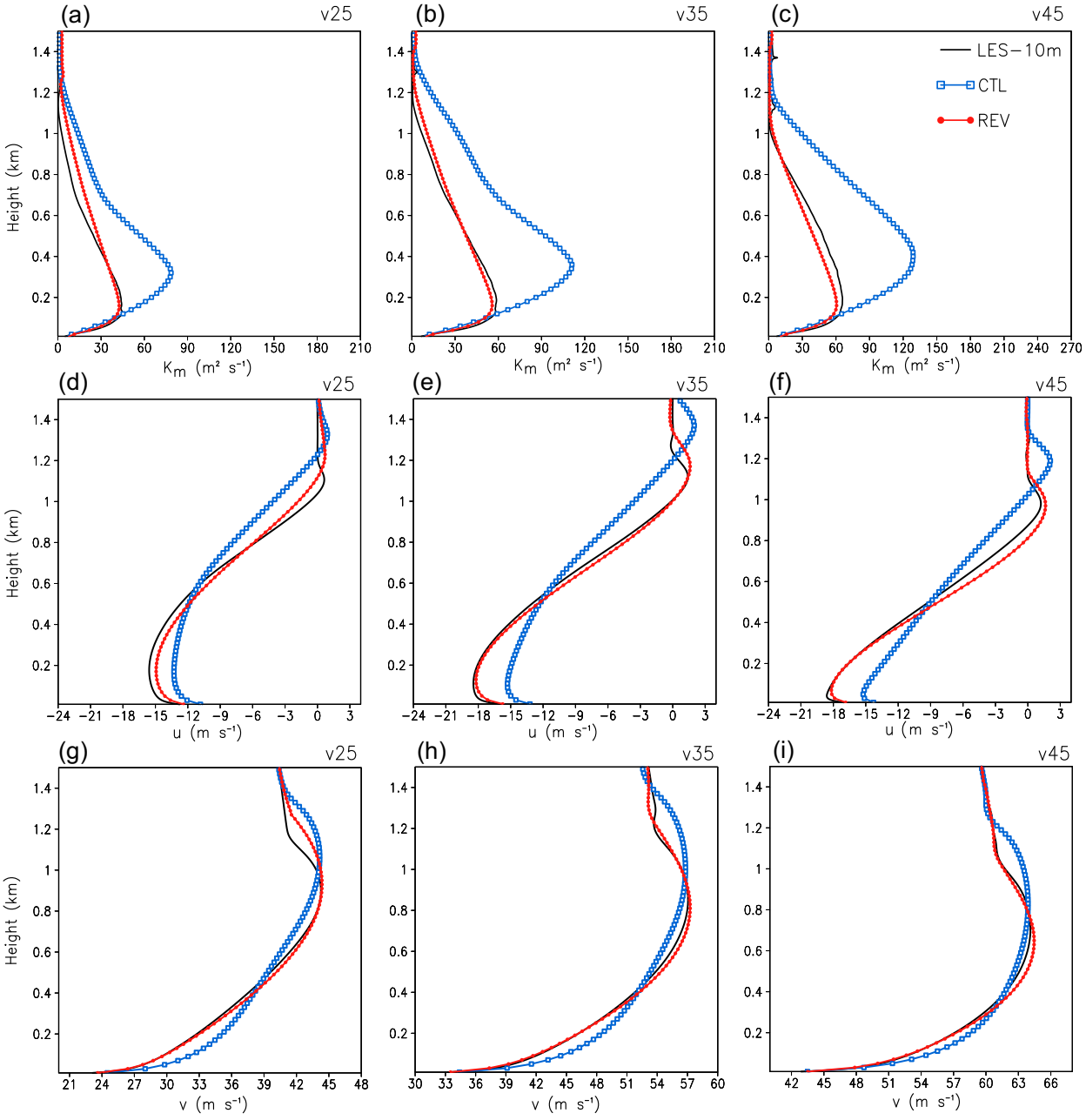

FIG. 5. As in Fig. 4, but for (a)–(c) K_m ($m^2\ s^{-1}$), (d)–(f) radial wind u ($m\ s^{-1}$), and (g)–(i) tangential wind v ($m\ s^{-1}$).

different high-wind conditions, and the level of maximum K_m in REV is closer to the surface than in CTL (Figs. 5a–c). Both of these characteristics in REV agree better with the LES results. With improved K_m profiles, the REV experiments reproduce the LES inflow layer depth (~1 km) and inflow strength (Figs. 5d–f). In comparison, the inflow layer in CTL is deeper than in LES in different high-wind conditions. Figures 5g–i further show that the tangential wind profiles in REV also agree well with the LES results. In short, the SCM tests demonstrate that the modified EDMF-TKE is capable of capturing similar profiles of turbulence properties and winds compared to LES in hurricane conditions, with a notably improved performance compared to the original EDMF-TKE.

As discussed in section 3, the modified EDMF-TKE incorporates four changes: 1) determining values of C_d and C_m that are needed to match the surface-layer and PBL parameterizations, 2) reducing the maximum allowable mixing length from 300 to 40 m, 3) implementing a new definition of the PBL height based on the bulk Richardson number that has been found to perform better in high-wind conditions, and 4)

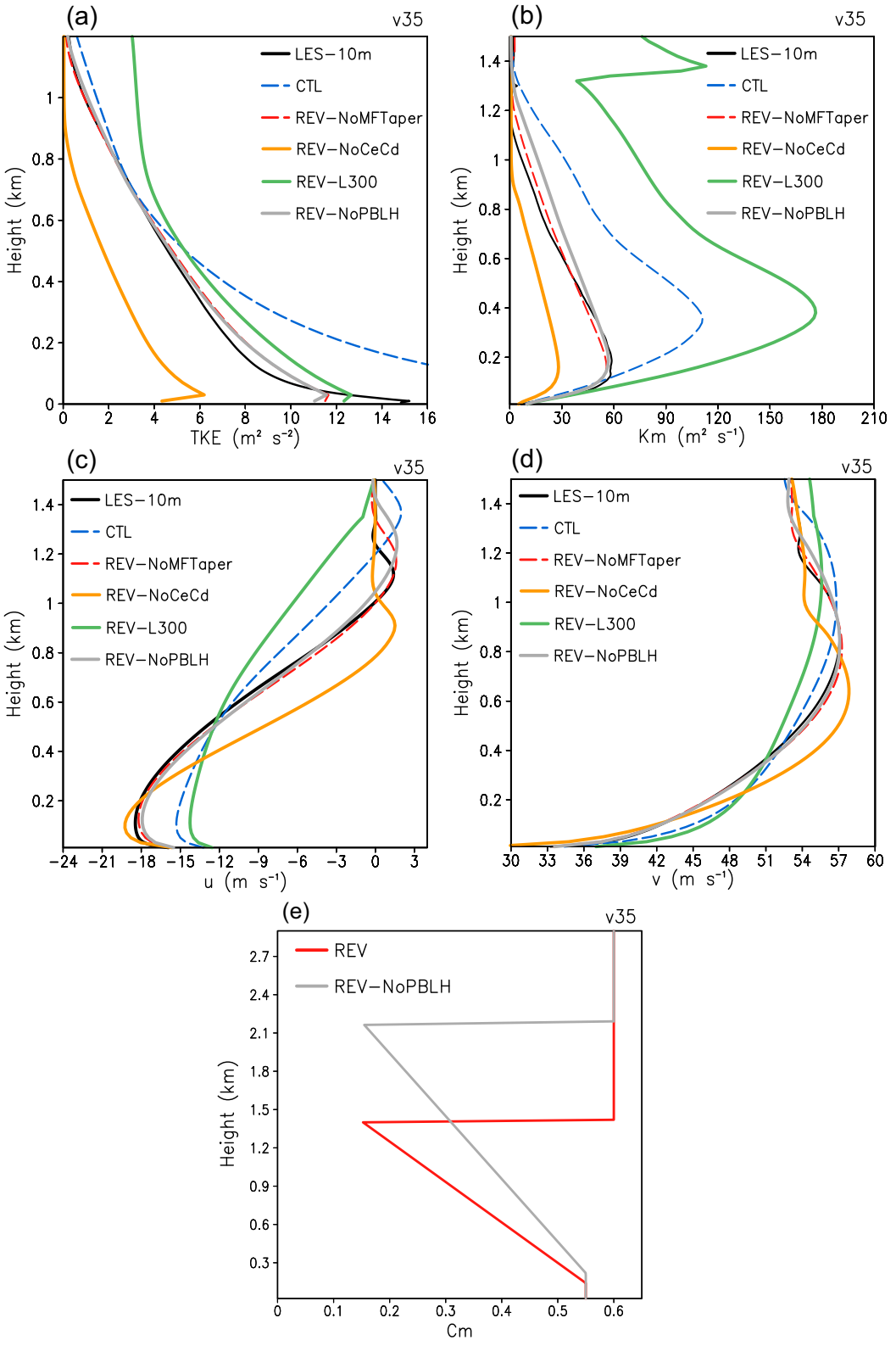

FIG. 6. (a)–(c) Vertical profile of (a) TKE ($m^2\ s^{-2}$), (b) K_m ($m^2\ s^{-1}$), (c) radial wind u ($m\ s^{-1}$), and (d) tangential wind v from LES (black line), CTL (dashed blue), and REV-based sensitivity tests for V35. The red, orange, green, and gray lines denote the REV experiment except changes to nonlocal mass fluxes are removed, changes to the C_d and C_m are removed, changes to the maximum allowable l_k are removed, and changes to the PBL height definition are removed, respectively. (e) Vertical profile of c_m from the REV experiment (red) and the REV-based sensitivity test excluding the changes to PBL height definition (gray) for V35.

tapering and then turning off mass fluxes from the nonlocal portion of the PBL scheme in high-wind conditions. As the four changes are in tandem with each other and the results in REV show their combined effect, we further examine which changes have the largest impact on the improvements. We perform four additional SCM tests based on REV by removing one of the four changes in each test. Figure 6 compares the results of these SCM tests against the LES for V35. The SCM tests without the changes to mass fluxes (dashed red line in Figs. 6a–d) match well with the LES results. This finding is attributable to the fact that the mass-flux parameterization is not activated with $\zeta \approx -1 \times 10^{-3}$ for V35 and also for V45 and V25 experiments, and stratocumulus-top driven mass fluxes [third term on the right-hand side of Eq. (A1)] are turned off for these SCM tests. Thus, *the dashed red lines in Figs. 6a–d are essentially the same as the REV experiment*. Due to the special model setup in SCM tests, one cannot draw the conclusion that mass fluxes in EDMF-TKE are unimportant in hurricane conditions, as three-dimensional CM1 tests indicate that the surface-driven mass fluxes and downgradient momentum fluxes can be of comparable magnitude at hurricane-force wind speeds (not shown).

In contrast, the most important of the four changes are changes 1 and 2, as removing either change 1 (orange line in Figs. 6a–d) or change 2 (green line in Figs. 6a–d) leads to notably different profiles of TKE, K_m, and winds compared to LES. Note that change 1 has a bigger impact on the TKE profile (Fig. 6a), whereas change 2 has a bigger impact on the K_m profile (Fig. 6b).

Figure 6e compares the profile of C_m between the REV (red line) and the REV-based sensitivity test excluding the changes to the PBL height (gray line). Including the changes to PBL height notably decreases the diagnosed boundary layer height (i.e., the level of minimum C_m) as well as the value of C_m within the diagnosed boundary layer height. As a consequence, comparison of the red and gray lines in Figs. 6b and 6c indicates that vertical mixing in terms of K_m and the inflow layer depth are slightly reduced using the new definition of the PBL height, although these differences are comparably much smaller than those produced by changes 1 and 2.

b. *Idealized three-dimensional simulations*

This section continues to assess the impact of the modified EDMF-TKE PBL scheme on the evolution of TCs by examining three-dimensional CM1 idealized numerical simulations. Figure 7 compares the evolution of TC intensity and size in the CTL and REV experiments. Compared to the CTL experiment, the simulated TC in REV starts to rapidly intensify at a slightly earlier time, the duration of rapid intensification (RI) in REV lasts slightly longer, and the REV TC attains a stronger intensity in terms of the 10-m maximum azimuthal-mean tangential wind after the RI period (Fig. 7a). The REV TC remains stronger than the CTL TC in the subsequent 6-day simulations. Additionally, the radius of the maximum wind (RMW) of the REV TC is ~20% smaller than that of the CTL TC during the simulation period (Fig. 7b). Nevertheless, the radius of gale-force wind (R17) in the two experiments is very similar, especially in the first 6 days, suggesting modifications to EDMF-TKE do not have a large impact on the outer-core size of the simulated TCs.

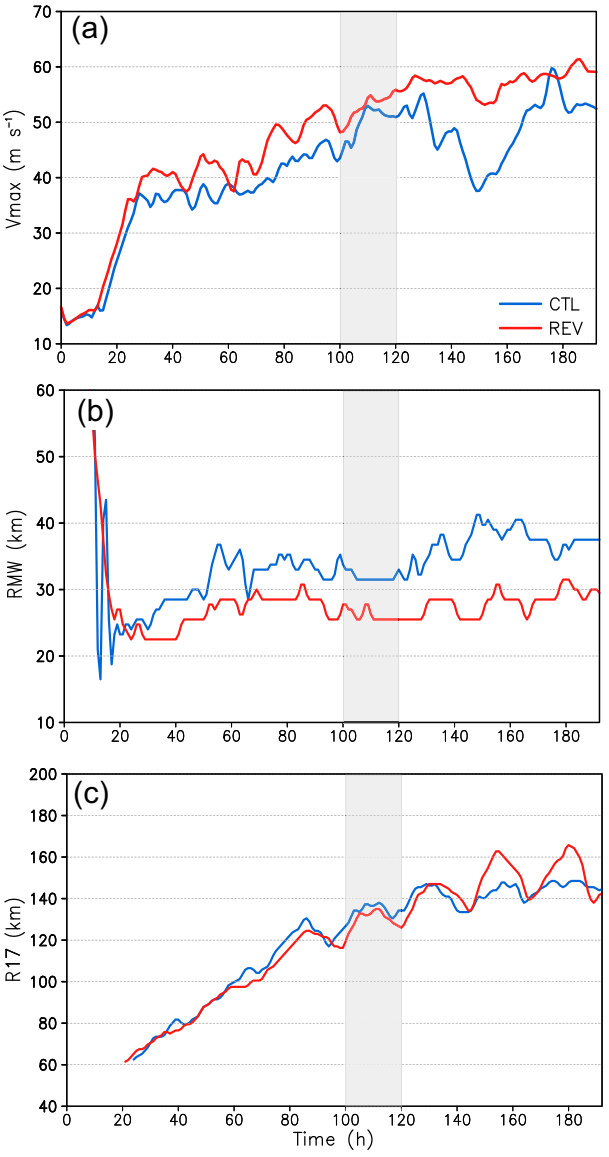

FIG. 7. Evolution of (a) 10-m maximum azimuthal-mean tangential wind V_m (m s^{-1}), (b) RMW (km), and (c) R17 (km) from CTL (blue) and REV (red) experiments. The light gray shaded box in (a)–(c) denotes an analysis period. R17 in (c) is shown after the simulated TC reaches hurricane intensity.

Figure 8 shows the Hovmöller diagram for the azimuthally averaged 1-km radar reflectivity and 10-m tangential wind. While the maximum radar reflectivity within the eyewall (r = 30–50 km) of the two TCs is comparable, large radar reflectivity of >45 dBZ in the eyewall appears at an earlier time and maintains for a longer time over the simulation

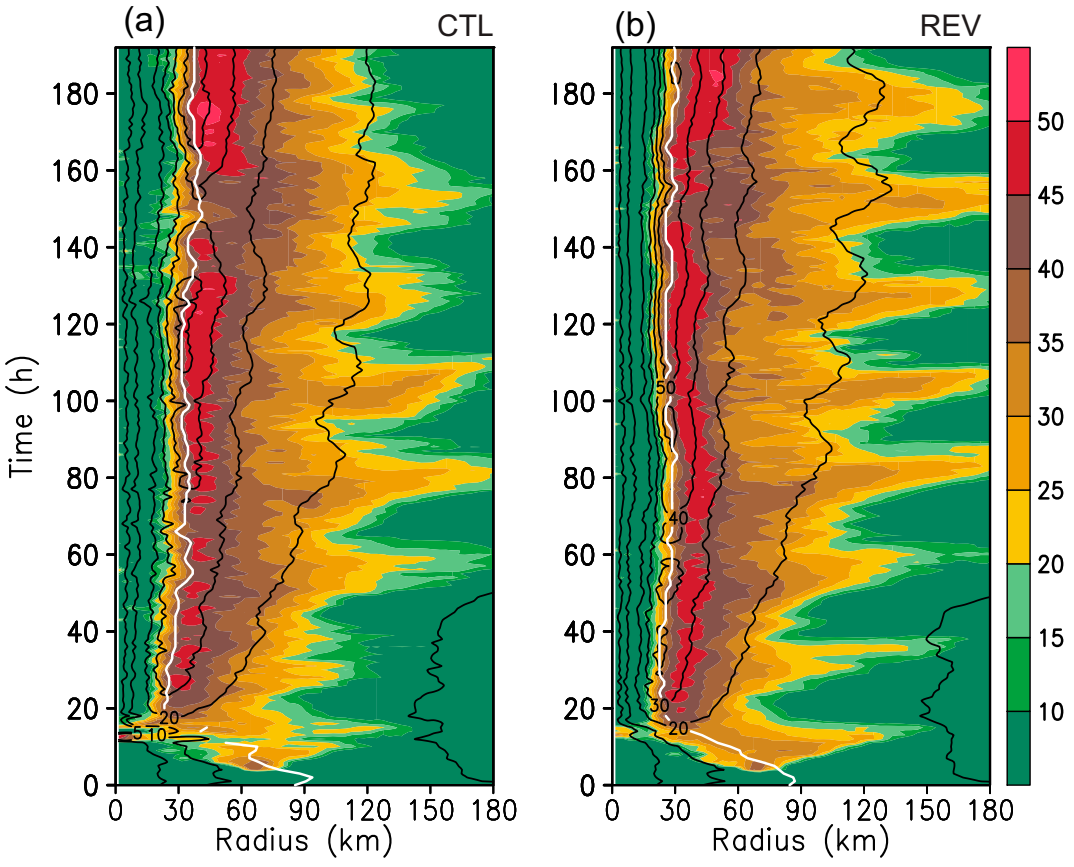

FIG. 8. Hovmöller diagram of azimuthally averaged 1-km radar reflectivity (shading; dBZ) and 10-m tangential wind (black contour with values of 5, 10, 20, 30, 40, 50, and 60 m s^{-1}) for (a) CTL and (b) REV experiments. The white line denotes the radius of the maximum wind (km).

period in REV than in CTL. This finding is in agreement with the stronger intensity of the REV TC.

To understand the differences in the TC intensity and structure between the two experiments, we examine radius–height plots of turbulence properties including TKE and K_m averaged over t = 100–120 h (Fig. 9). Over this period, TC intensity and RMW in the two experiments are comparable. One notable difference in the distribution of TKE between the two experiments is that the TKE column (>1 m^2 s^{-2}) in the eyewall region of the REV TC extends to higher levels than that of the CTL TC (Figs. 9a,b). The eyewall region is indicated by updrafts with $w > 1$ m s^{-1} (see the red contour in Figs. 9a,b). Given advection of TKE is not included in these simulations, differences in the depth of TKE column are attributable to the modifications to EDMF-TKE. Additionally, the REV TC has much smaller TKE values below 500 m height than the CTL TC (Fig. 9c), which is consistent with the findings from SCM tests (e.g., Figs. 4a–c); the difference in TKE attains its maximum near the surface of the eyewall region (>6 m^2 s^{-2}, Fig. 9c), where surface winds are the strongest. Differences in the K_m distribution between the two experiments resemble the differences in the TKE distribution, with the K_m column (>10 m^2 s^{-2}) in the eyewall of the REV TC extending to a slightly higher level (Figs. 9d–f). The REV TC has smaller K_m within the diagnosed h (the orange line in Figs. 9d–e) and above the near-surface layer than the CTL TC. In contrast, the REV TC has slightly larger K_m in the near-surface layer than the CTL TC (Fig. 9f). These findings are quite similar to the results from SCM tests (Figs. 5a–c), where K_m in the near-surface layer in REV agrees better with the LES results.

Figures 9a and 9b also compare the diagnosed h (the solid orange line; see definition in the appendix) and h_{Ric} (the dashed gray line) between the two experiments. With the inclusion of a modified PBL height definition, the diagnosed h_{Ric} in REV is ~600 m shallower than that in CTL. Using h_{Ric} as a first guess, h is further determined by taking the smaller value between h_{Ric} and the diagnosed boundary layer height of updraft velocity w_u = 0. The reduced h compared to h_{Ric} indicates that the diagnosed boundary layer height of w_u = 0 is shallower than h_{Ric}. Nevertheless, h in REV remains shallower than that in CTL, which is expected based on the SCM tests, and the largest difference of ~1 km appears within 1–2 × RMW.

The eddy viscosity K_m in the boundary layer is known to affect boundary layer inflow structure, with smaller K_m

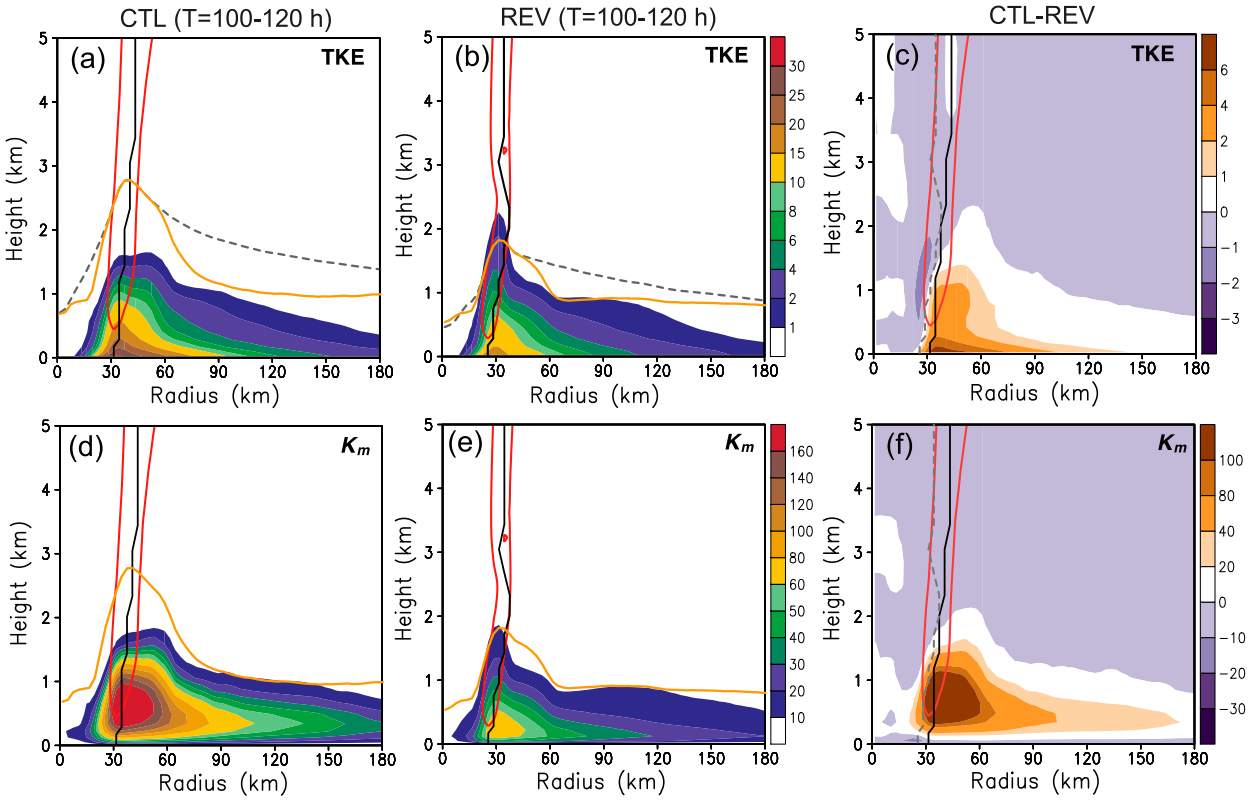

FIG. 9. (a),(b) Radial–height plot of azimuthally averaged TKE (shading; $m^2\ s^{-2}$) averaged over t = 100–120 h for CTL and REV experiments, respectively. The difference in the distribution of TKE (i.e., CTL − REV) is shown in (c). (d)–(f) As in (a)–(c), but for K_m (shading; $m^2\ s^{-1}$). In each panel, the red contour denotes w = 1 m s^{-1}, and the black line denotes the mean RMW. In (c) and (f), the w contours are from CTL, and the black and dashed gray lines denote RMW from CTL and REV, respectively. The orange line in (a) and (b) and (d) and (e) denotes the mean h. In (a) and (b), the dashed gray line denotes h_{Ric}.

typically resulting in stronger inflow strength and a shallower inflow depth (e.g., Foster 2009; Gopalakrishnan et al. 2013; Zhang et al. 2015). This finding is supported by a comparison of inflow structure averaged over t = 100–120 h in Figs. 10a and 10b. The inflow layer depth (inflow depth indicated by $u = -1$ m s^{-1}) of the REV TC is ~500 m shallower than that of the CTL TC within 1–3 × RMW. The REV TC has stronger boundary layer inflow than the CTL TC beneath the eyewall, while it is difficult to see the differences clearly radially outward due to the differences in the RMW of the CTL and REV TCs over this period (Figs. 10a,b). Given this limitation, we adopt another insightful measure of inflow strength, i.e., surface inflow angle, defined as $\tan^{-1}(u_{10}/v_{10})$, where u_{10} and v_{10} are the radial and tangential velocities at 10-m height, respectively.

Figure 10c shows the composite radial profile of inflow angle averaged over t = 100–120 h. The REV TC has larger inflow angles than the CTL TC outside the RMW, with the largest differences of ~4°, suggesting inflow outside the RMW is stronger in REV. For reference, Figs. 10c and 10d also show a radial profile of observed inflow angle based on a composite of 1600 global positioning system (GPS) dropsondes collected in 18 different hurricanes (Zhang and Uhlhorn 2012). The median storm intensity for the dropsonde data is 56.7 m s^{-1}, which fits in the category-3 hurricane intensity and is similar to the intensity of the simulated TCs over t = 100–120 h (Fig. 10c). Possibly due to the similar TC intensity, the inflow angle in both CTL and REV is encouragingly comparable to observations over t = 100–120 h. To examine the robustness of this finding as well as the variability of inflow angle to TC intensity, radial profiles of inflow angle over t = 25–45 h are also shown in Fig. 10d. Over this period, the mean TC intensity in terms of the 10-m maximum tangential wind is ~40 m s^{-1} (category-1 hurricane) in both experiments. Compared to the results over t = 100–120 h, the magnitude of inflow angle increases by ~2°–3° within 1–3 × RMW in REV while it generally decreases by 2°–3° outside the RMW in CTL over t = 25–45 h. Therefore, the inflow angle in REV becomes even larger than in CTL over t = 25–45 h, with the largest differences of ~10° within 1–2 × RMW. Additionally, compared to the results over t = 100–120 h, the peak inflow angle in CTL is shifted radially outward to 2 × RMW over t = 25–45 h (Fig. 10b); the notable weakening of radial inflow within 1–2 × RMW may account for a tendency of RMW expansion in CTL over the same period (Fig. 6b). These findings suggest that radial profiles of inflow angle depend on TC intensity and

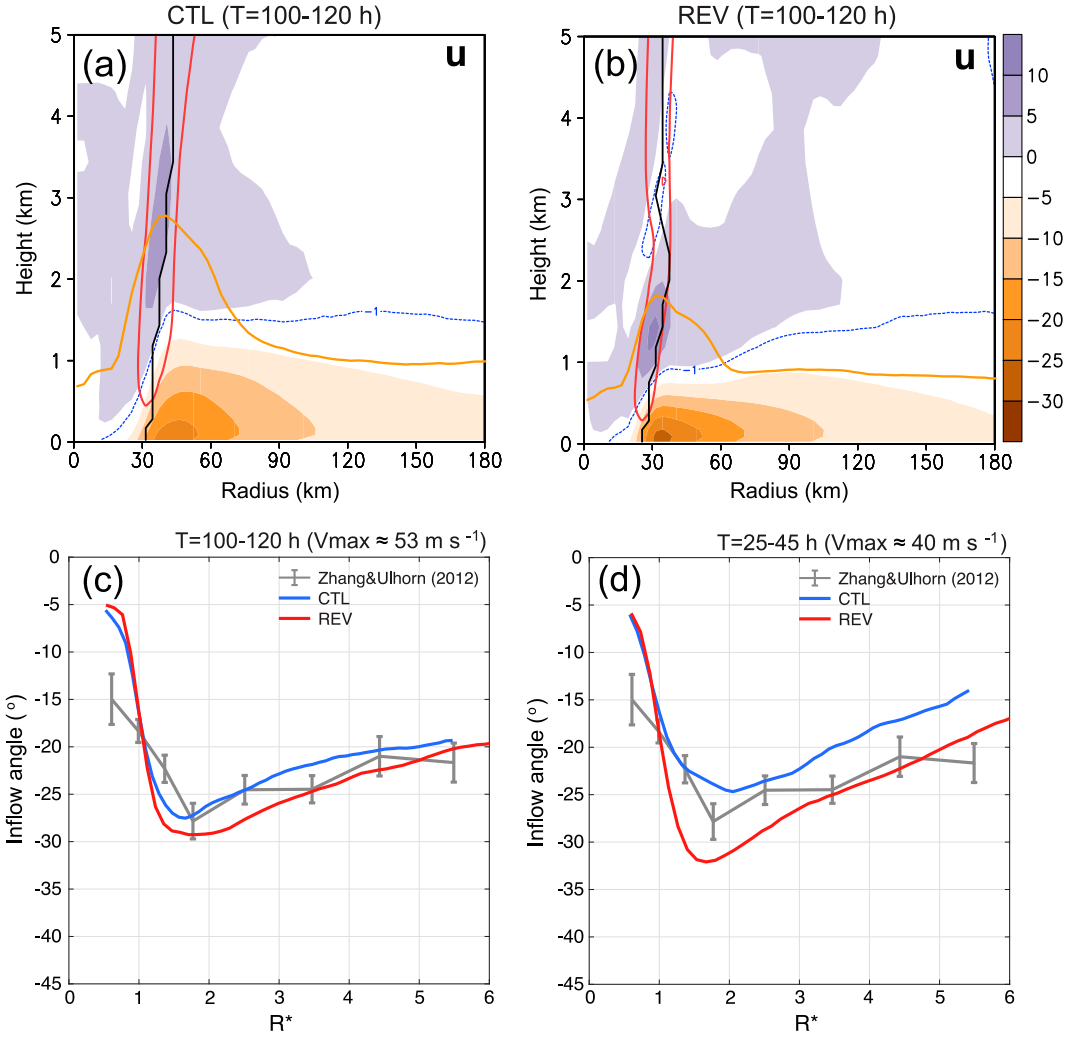

FIG. 10. (a),(b) Radial–height plot of azimuthally averaged radial velocity u (shading; m s^{-1}) averaged over t = 100–120 h for CTL and REV experiments, respectively. The red contour denotes w = 1 m s^{-1}, and the black line denotes the mean RMW. The orange line denotes the mean h, and the dashed blue line denotes u = −1 m s^{-1} (c),(d) Composite 10-m radial profile of inflow angle (°) as a function of normalized radius R^* (=R/RMW) for CTL (blue) and REV (red) over t = 100–120 h in (c) and t = 25–45 h in (d). The 10-m radial profile of inflow angle from a dropsonde composite of category-1–5 hurricanes (Zhang and Uhlhorn 2012) is shown for a reference (gray); the gray bar denotes 95% confidence intervals. The maximum intensity of simulated TCs averaged over each period is shown on the top of (c) and (d).

structure. Examining the variability of inflow angle to TC intensity and structural changes using observations or modeling output will be an interesting topic to pursue for future work.

In short, the stronger boundary layer inflow in REV contributes to stronger convergence beneath the eyewall, which contributes to a more sustained eyewall convective activity in REV (Fig. 8b). The relationship of the enhanced convergence within the eyewall and stronger diabatic heating was also suggested in an observational study of Hurricane Allen (1980) (see Fig. 15 in Marks 1985). These physical processes account for the stronger TC with a smaller RMW in REV than in CTL.

c. *HAFS forecasts of Hurricane Michael (2018)*

To test the robustness of the findings from idealized simulations, we examine two sets of 5-member ensemble HAFS forecasts of Hurricane Michael (2018) using the original and modified EDMF-TKE schemes, respectively. Figure 11 compares the evolution of TC track, intensity, and RMW from the CTL (blue lines) and REV (red lines) experiments against best track data from NOAA's National Hurricane Center (dashed gray line). Figures 11a and 11b suggest that compared to best track data the simulated TCs in the two sets of ensemble experiments move faster and thereby make landfall at an earlier time (t ≈ 60 h) than in the best track (t ≈ 72 h).

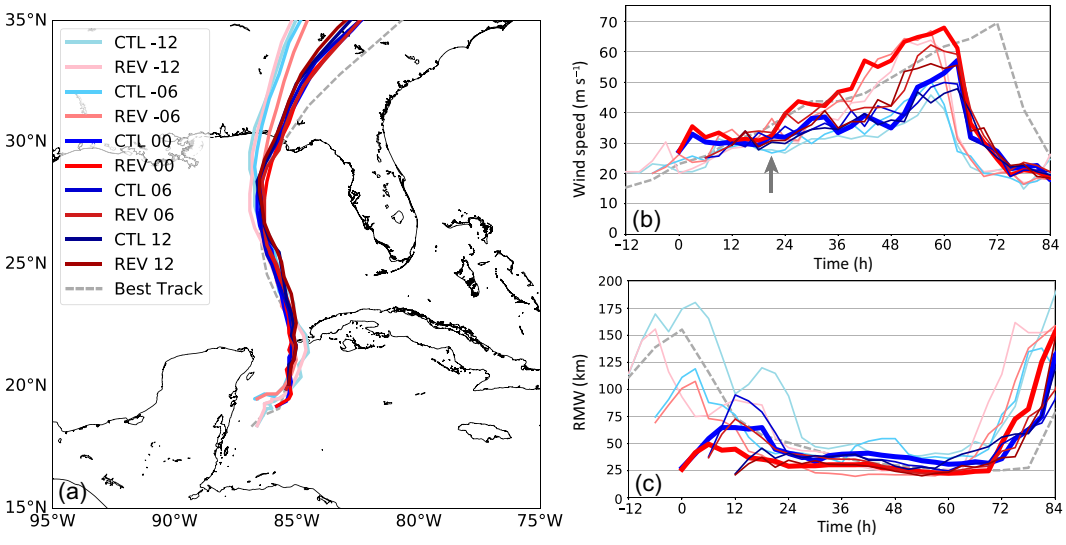

FIG. 11. Two sets of 5-member ensemble HAFS forecasts of Hurricane Michael (2018) initialized at −12, −6, 0, +6, and +12 h relative to 1800 UTC 7 Oct, respectively, showing evolution of (a) TC track, (b) 10-m maximum wind (m s^{-1}), and (c) RMW (km). The dashed gray line denotes best track; blue and red lines denote CTL and REV experiments, respectively. The thick red and blue lines in (b) and (c) denote the experiments initialized at 1800 UTC 7 Oct, and the gray arrow in (b) denotes the bifurcation point of the two experiments.

However, Fig. 11b shows that the REV TCs remain stronger than the CTL TCs prior to landfall, as the CTL TCs generally remain in steady state or intensify very slowly until t = 48 h. The averaged maximum intensity of the REV TCs is ~63 m s^{-1}, approximately 13 m s^{-1} stronger than that of the CTL TCs, but is very close to the maximum intensity indicated by the best track (~70 m s^{-1}). Prior to landfall, the contraction of RMW is more notable in REV than in CTL (Fig. 11c), especially early in these forecasts; the smaller RMW in REV agrees better with the best track data. The R17 is very similar between the two sets of ensemble experiments and is not shown.

Figure 12 shows the CTL and REV experiments initialized at 1800 UTC 7 October 2018 and compares their composite radial wind structure over t = 18–24 h, which centers on the bifurcation point for the evolution of TC intensity, after which the REV TC intensifies faster than the CTL TC (see Fig. 11b). Clearly, the REV TC has stronger boundary layer inflow than the CTL TC, especially within 1–3 × RMW (see Fig. 12c), which is particularly consistent with the findings of the idealized simulations over t = 25–45 h (Fig. 10d), when the simulated TCs have comparable intensity. The stronger boundary layer inflow and smaller RMW contribute to the earlier RI onset timing in REV, which is consistent with the findings in

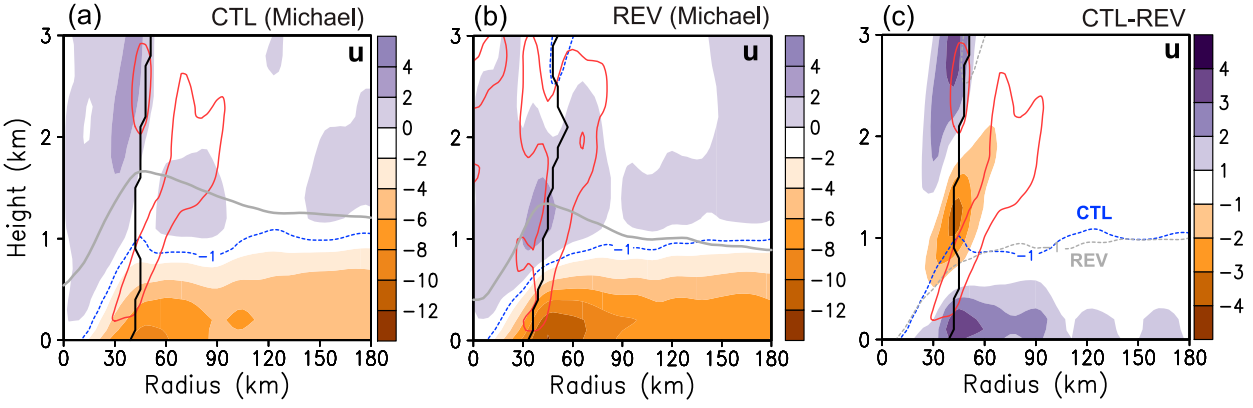

FIG. 12. Radial–height plot of azimuthally averaged radial wind (shading; m s^{-1}) averaged over t = 18–24 h for the (a) CTL and (b) REV experiments of Hurricane Michael (2018) initialized at 1800 UTC 7 Oct. (c) The difference in radial winds (i.e., CTL − REV). In (a) and (b), the dashed blue line denotes u = −1 m s^{-1}, and the gray line denotes h_{Ric}. The red contour in (a) and (b) denotes w = 0.3 m s^{-1}, and the black line denotes the mean RMW. In (c), the RMW and w contours are from CTL, and the dashed blue and gray lines denote the inflow layer depth from CTL and REV, respectively.

Chen et al. (2018). Comparison of the diagnosed h_{Ric} (gray lines in Figs. 12a,b) shows that h_{Ric} is reduced by 300–500 m in REV than in CTL, reminiscent of results of the idealized simulations (e.g., Figs. 9a,b), which would contribute to a reduction of the vertical turbulent mixing in REV as discussed in section 3b. Comparison of inflow layer depth, indicated by dashed blue and gray lines in Fig. 12c, shows that the inflow layer depth in REV is similar between the two experiments except near the RMW, where the inflow layer depth in REV is 200–300 m shallower than in CTL. The relatively large discrepancy in the inflow layer depth near the RMW is also seen in Figs. 10a and 10b.

In summary, differences in TC intensity, size, boundary layer height, and inflow structure from two sets of ensemble HAFS forecasts are generally consistent with those from idealized 3D simulations, confirming that the modified EDMF-TKE tends to produce stronger boundary layer inflow, stronger TC intensity, and a smaller RMW than the original EDMF-TKE.

5. Conclusions

A TKE-based eddy-diffusivity mass-flux (EDMF) PBL scheme (EDMF-TKE) is used in NOAA's Global Forecast System (GFS) model as well as the next-generation hurricane forecast model, the Hurricane Analysis and Forecast System (HAFS). Given this PBL scheme is not specifically designed for the hurricane boundary layer, this study evaluates and improves a new version of this PBL scheme (targeted for version 17 of GFS model) in hurricane conditions using a recently developed evaluation framework proposed by Chen et al. (2021a).

Evaluation results show that the original EDMF-TKE substantially overestimates TKE below 500-m height in hurricane conditions compared to LES; additionally, EDMF-TKE overpredicts the diagnosed boundary layer height and inflow layer depth. To improve the results, four changes are made: 1) the coefficients used to determine eddy viscosity and TKE dissipation are modified to ensure a match between the PBL and surface-layer parameterizations; 2) the maximum allowable value of mixing length is reduced from 300 to 40 m based on LES results and observational estimates; 3) a different PBL height definition is adopted that works well in the hurricane boundary layer; and 4) nonlocal turbulent mass fluxes in high-wind conditions are reduced, given the impact of strong vertical wind shear on damping rising thermal plumes. SCM tests using the modified EDMF-TKE demonstrate that vertical profiles of TKE, eddy viscosity, and winds are substantially improved and match well with the LES results. Among the four changes, the first two changes were found to have the largest impact on the improvements.

Comparisons of three-dimensional idealized simulations using the original (i.e., the CTL experiment) and modified EDMF-TKE (i.e., the REV experiment) show that the modified EDMF-TKE tends to produces a stronger vortex with a smaller radius of maximum wind (RMW). However, these experiments produce a similar radius of gale-force wind (R17), suggesting the TC outer-core size is unaffected. The smaller eddy viscosity in the boundary layer in REV results in stronger boundary layer inflow outside the RMW. The enhanced convergence beneath the eyewall is thereby enhanced in REV, supporting a more sustained convective activity in the eyewall. Two sets of ensemble HAFS forecasts of Hurricane Michael (2018) using the two PBL schemes nicely agree with the results of idealized simulations.

As a concluding note, the modified EDMF-TKE substantially improves the turbulence properties and wind profiles in the hurricane boundary layer, and also shows encouraging promise to improve the forecasts of rapid intensification of hurricanes under sheared environments. Future work will further assess the impact of the modified EDMF-TKE on the model forecast skills of hurricane intensity/structure change by testing more cases over a wide range of intensities during the 2021 Atlantic hurricane season.

Acknowledgments. We would like to acknowledge high-performance computing support from Cheyenne (doi:10.5065/D6RX99HX) provided by NCAR's Computational and Information Systems Laboratory, sponsored by the National Science Foundation. The authors appreciate Dr. Jun Zhang for generously sharing the inflow angle data and Dr. Scott Braun for the conversation regarding the new definition of PBL height. The constructive suggestions and comments from Dr. Kyle Ahern, Dr. Gus Alaka, and three anonymous reviewers improved the clarity of the method and quality of the analysis. Xiaomin Chen is supported by Award NA21OAR4320190 to the Northern Gulf Institute at Mississippi State University from NOAA's Office of Oceanic and Atmospheric Research, U.S. Department of Commerce. George Bryan is supported by the National Center for Atmospheric Research, which is a major facility sponsored by the National Science Foundation under Cooperative Agreement 1852977, and by Office of Naval Research Grant N00014-20-1-2071.

Data availability statement. The LES and single-column modeling experiments using the CM1 model are available on NCAR's Cheyenne supercomputer. The HAFS simulations of Hurricane Michael (2018) are available on the NOAA RDHPCS computer system, or by request.

APPENDIX

A Brief Overview of the EDMF-TKE PBL Scheme

EDMF-TKE is a 1.5-order PBL scheme developed by Han and Bretherton (2019). The vertical turbulent flux $\overline{w'\phi'}$ in EDMF-TKE is parameterized as

$$\overline{w'\phi'} = -K_{\phi}\left(\frac{\partial\overline{\phi}}{\partial z}\right) + M_u\left(\phi_u - \overline{\phi}\right)\Big|_{\mathrm{sfc}} + M_d\left(\phi_d - \overline{\phi}\right)\Big|_{\mathrm{Sc}}, \quad \text{(A1)}$$

where ϕ denotes one prognostic variable (i.e., potential temperature, winds, and scalars including TKE). The overbar denotes the horizontal average over a grid cell. The term M is mass flux; the subscripts "u" and "d" denote updraft and downdraft properties, respectively; "sfc" and "Sc" denote surface driven and stratocumulus-top driven,

respectively. The terms on the right-hand side (rhs) of (A1) are downgradient turbulent flux, surface-driven mass flux, and stratocumulus-top-driven mass flux, respectively. The eddy diffusivity K_ϕ is parameterized as

$$K_\phi = c_\phi l_k \sqrt{\bar{e}}, \tag{A2}$$

where e denotes parameterized (i.e., subgrid) TKE, c_ϕ is a stability coefficient, and l_k is mixing length. The stability coefficient for momentum c_m relates to the stability coefficient for heat c_h by a Prandtl number P_r: $c_m = c_h P_r$. Subgrid TKE is a prognostic variable that is determined by a simplified version of the TKE budget equation:

$$\frac{\partial \bar{e}}{\partial t} = \frac{g}{\bar{\theta}_v}\overline{w'\theta'_v} - \left(\overline{u'w'}\frac{\partial \bar{u}}{\partial z} + \overline{v'w'}\frac{\partial \bar{v}}{\partial z}\right) - \frac{\partial\left(\overline{w'\bar{e}} + \frac{1}{\rho}\overline{w'p'}\right)}{\partial z} - D, \tag{A3}$$

where θ_v is virtual potential temperature; u, v, and w are zonal, meridional, and vertical winds, respectively; g is the gravitational parameter; and ρ is air density. In the design of one-dimensional (1D) PBL schemes for mesoscale simulations where horizontal grid spacings are typically greater than the scale of energy-containing eddies, subgrid-scale turbulent processes are assumed horizontally homogeneous and vertical advection of subgrid-scale processes are negligible (see Stull 1988, p. 152). Shear production terms due to horizontal gradients of u, v, and w are also neglected. The TKE advection term is not included in (A3)[A1] for simplicity, and we have investigated the role of TKE advection in a separate study (i.e., Chen and Bryan 2021). Terms on the rhs of (A3) are buoyancy production/sink, shear production, turbulence transport term, and parameterized dissipation of TKE, respectively. Based on (A1), the turbulence transport term is parameterized as

$$-\frac{\partial}{\partial z}\left(\overline{w'\bar{e}} + \frac{1}{\rho}\overline{w'p'}\right) = -\frac{\partial}{\partial z}\left[-K_e\frac{\partial \bar{e}}{\partial z} + M_u(e_u - \bar{e})\Big|_{\text{sfc}} + M_d(e_d - \bar{e})\Big|_{\text{Sc}}\right], \tag{A4}$$

where K_e is eddy diffusivity for TKE. It is assumed $K_e = K_h$ in EDMF-TKE, where K_h is eddy diffusivity for heat and moisture. The dissipation of TKE is parameterized as

$$D = C_d\frac{\bar{e}^{3/2}}{l_d}, \tag{A5}$$

which is (6) from Han and Bretherton (2019) but with the exponent corrected (i.e., $\bar{e}^{3/2}$ instead of $\bar{e}^{-3/2}$). The term C_d is a dissipation coefficient, and l_d denotes turbulent dissipation length scale.

The formulation of mixing length l_k is determined by a harmonic average of two length scales:

$$l_k^{-1} = l_s^{-1} + l_{\text{BL}}^{-1}. \tag{A6}$$

The surface length scale l_s is defined as $l_s = kz\left[a_1 + a_2(z/L)\right]^{a_3}$, following Nakanish (2001), where k is the von Kármán constant (= 0.4), L is the Monin–Obukhov length, and a_1, a_2, and a_3 are stability-dependent coefficients. The term l_{BL} denotes the BouLac length scale. Following Bougeault and Lacarrere (1989), l_{BL} and l_d are determined by

$$l_{\text{BL}} = \min(l_{\text{up}}, l_{\text{down}}),\ l_d = \left(l_{\text{up}}\ l_{\text{down}}\right)^{1/2}, \tag{A7}$$

where l_{up} and l_{down} are the maximum possible distance traveled by an air parcel due to the loss of TKE via effects of buoyancy and vertical wind shear such that

$$\int_z^{z+l_{\text{up}}}\left\{\frac{g}{\bar{\theta}_v(z)}\left[\bar{\theta}_v(z') - \bar{\theta}_v(z)\right] + C_0\sqrt{\bar{e}}S(z')\right\}dz' = \bar{e}(z),$$

$$\int_{z-l_{\text{down}}}^{z}\left\{\frac{g}{\bar{\theta}_v(z)}\left[\bar{\theta}_v(z) - \bar{\theta}_v(z')\right] + C_0\sqrt{\bar{e}}S(z')\right\}dz' = \bar{e}(z), \tag{A8}$$

where $C_0 = 0.2$ and $S(z')$ is the local shear. Of note, the effect of vertical wind shear based on Rodier et al. (2017) was recently included in EDMF-TKE.

One key variable to diagnose in EDMF-TKE is the boundary layer height h, which determines the entrainment rate in the prognostic equation for updraft velocity w_u [related to M_u, see (14) in Han and Bretherton 2019] as well as the vertical profile of c_m and c_h (see discussions in section 3a). The height h is determined by the smaller value of the height of $w_u = 0$ and the height invoking a critical bulk Richardson number (h_{Ric}, Troen and Mahrt 1986). The h_{Ric} is determined by

$$h_{\text{Ric}} = \text{Ric}\frac{\left(u_h^2 + v_h^2\right)\theta_{va}}{g(\theta_{vh} - \theta_{vs})}, \tag{A9}$$

where u_h, v_h, and θ_{vh} are zonal and meridional winds, and virtual potential temperature at $z = h_{\text{Ric}}$, respectively. The term θ_{va} is the virtual potential temperature at the lowest model level, and the temperature near the surface θ_{vs} is defined as $\theta_{vs} = \theta_{va} + \theta_T$, where θ_T is virtual temperature excess near the surface. For unstable surface-layer conditions (with positive surface enthalpy fluxes), Ric = 0.25. For more details of the EDMF-TKE PBL scheme, we refer interested readers to Han and Bretherton (2019).

[A1] Equation (A3) slightly differs from (4) in Han and Bretherton (2019) in that $d\bar{e}/dt$ is used in their (4).

REFERENCES

Arakawa, A., J. H. Jung, and C. M. Wu, 2011: Toward unification of the multiscale modeling of the atmosphere. *Atmos. Chem. Phys.*, **11**, 3731–3742, https://doi.org/10.5194/acp-11-3731-2011.

Berg, J., E. G. Patton, and P. P. Sullivan, 2020: Large-eddy simulation of conditionally neutral boundary layers: A mesh resolution sensitivity study. *J. Atmos. Sci.*, **77**, 1969–1991, https://doi.org/10.1175/JAS-D-19-0252.1.

Beven, J. L., II, R. Berg, and A. Hagen, 2019: National Hurricane Center tropical cyclone report: Hurricane Michael (7–11 October 2018). NOAA/NHC Tech. Rep. AL142018, 86 pp., https://www.nhc.noaa.gov/data/tcr/AL142018_Michael.pdf.

Bleck, R., 2002: An oceanic general circulation model framed in hybrid isopycnic–Cartesian coordinates. *Ocean Modell.*, **4**, 55–88, https://doi.org/10.1016/S1463-5003(01)00012-9.

Bougeault, P., and P. Lacarrere, 1989: Parameterization of orography-induced turbulence in a mesobeta-scale model. *Mon. Wea. Rev.*, **117**, 1872–1890, https://doi.org/10.1175/1520-0493(1989)117<1872:POOITI>2.0.CO;2.

Braun, S. A., and W.-K. Tao, 2000: Sensitivity of high-resolution simulations of Hurricane Bob (1991) to planetary boundary layer parameterizations. *Mon. Wea. Rev.*, **128**, 3941–3961, https://doi.org/10.1175/1520-0493(2000)129<3941:SOHRSO>2.0.CO;2.

Bryan, G. H., 2012: Effects of surface exchange coefficients and turbulence length scales on the intensity and structure of numerically simulated hurricanes. *Mon. Wea. Rev.*, **140**, 1125–1143, https://doi.org/10.1175/MWR-D-11-00231.1.

——, and J. M. Fritsch, 2002: A benchmark simulation for moist nonhydrostatic numerical models. *Mon. Wea. Rev.*, **130**, 2917–2928, https://doi.org/10.1175/1520-0493(2002)130<2917:ABSFMN>2.0.CO;2.

——, R. P. Worsnop, J. K. Lundquist, and J. A. Zhang, 2017: A simple method for simulating wind profiles in the boundary layer of tropical cyclones. *Bound.-Layer Meteor.*, **162**, 475–502, https://doi.org/10.1007/s10546-016-0207-0.

Bu, Y. P., R. G. Fovell, and K. L. Corbosiero, 2017: The influences of boundary layer mixing and cloud-radiative forcing on tropical cyclone size. *J. Atmos. Sci.*, **74**, 1273–1292, https://doi.org/10.1175/JAS-D-16-0231.1.

Chen, X., and G. Bryan, 2021: Role of advection of parameterized turbulence kinetic energy in idealized tropical cyclone simulations. *J. Atmos. Sci.*, **78**, 3593–3611, https://doi.org/10.1175/JAS-D-21-0088.1.

——, M. Xue, and J. Fang, 2018: Rapid intensification of Typhoon Mujigae (2015) under different sea surface temperatures: Structural changes leading to rapid intensification. *J. Atmos. Sci.*, **75**, 4313–4335, https://doi.org/10.1175/JAS-D-18-0017.1.

——, G. H. Bryan, J. A. Zhang, J. J. Cione, and F. D. Marks, 2021a: A framework for simulating the tropical cyclone boundary layer using large-eddy simulation and its use in evaluating PBL parameterizations. *J. Atmos. Sci.*, **78**, 3559–3574, https://doi.org/10.1175/JAS-D-20-0227.1.

——, M. Xue, B. Zhou, J. Fang, J. A. Zhang, and F. D. Marks, 2021b: Effect of scale-aware planetary boundary layer schemes on tropical cyclone intensification and structural changes in the gray zone. *Mon. Wea. Rev.*, **149**, 2079–2095, https://doi.org/10.1175/MWR-D-20-0297.1.

Dong, J., and Coauthors, 2020: The evaluation of real-time Hurricane Analysis and Forecast System (HAFS) Stand-Alone Regional (SAR) model performance in 2019 Atlantic hurricane season. *Atmosphere*, **11**, 617, https://doi.org/10.3390/atmos11060617.

Foster, R. C., 2009: Boundary-layer similarity under an axisymmetric, gradient wind vortex. *Bound.-Layer Meteor.*, **131**, 321–344, https://doi.org/10.1007/s10546-009-9379-1.

——, 2013: Signature of large aspect ratio roll vortices in synthetic aperture radar images of tropical cyclones. *Oceanography*, **26**, 58–67, https://doi.org/10.5670/oceanog.2013.31.

Gopalakrishnan, S. G., F. Marks, J. A. Zhang, X. Zhang, J.-W. Bao, and V. Tallapragada, 2013: A study of the impacts of vertical diffusion on the structure and intensity of the tropical cyclones using the high-resolution HWRF system. *J. Atmos. Sci.*, **70**, 524–541, https://doi.org/10.1175/JAS-D-11-0340.1.

Grant, A. L. M., 1992: The structure of turbulence in the near-neutral atmospheric boundary layer. *J. Atmos. Sci.*, **49**, 226–239, https://doi.org/10.1175/1520-0469(1992)049<0226:TSOTIT>2.0.CO;2.

Han, J., and C. S. Bretherton, 2019: TKE-based moist Eddy-Diffusivity Mass-Flux (EDMF) parameterization for vertical turbulent mixing. *Wea. Forecasting*, **34**, 869–886, https://doi.org/10.1175/WAF-D-18-0146.1.

Hazelton, A. T., X. Zhang, W. Ramstrom, S. Gopalakrishan, F. D. Marks, and J. A. Zhang, 2020: High-resolution ensemble HFV3 forecasts of Hurricane Michael (2018): Rapid intensification in shear. *Mon. Wea. Rev.*, **148**, 2009–2032, https://doi.org/10.1175/MWR-D-19-0275.1.

——, and Coauthors, 2021: 2019 Atlantic hurricane forecasts from the global-nested Hurricane Analysis and Forecast System: Composite statistics and key events. *Wea. Forecasting*, **36**, 519–538, https://doi.org/10.1175/WAF-D-20-0044.1.

Hill, K. A., and G. M. Lackmann, 2009: Analysis of idealized tropical cyclone simulations using the Weather Research and Forecasting Model: Sensitivity to turbulence parameterization and grid spacing. *Mon. Wea. Rev.*, **137**, 745–765, https://doi.org/10.1175/2008MWR2220.1.

Kepert, J. D., 2012: Choosing a boundary layer parameterization for tropical cyclone modeling. *Mon. Wea. Rev.*, **140**, 1427–1445, https://doi.org/10.1175/MWR-D-11-00217.1.

Marks, F. D., Jr., 1985: Evolution of the structure of precipitation in Hurricane Allen (1980). *Mon. Wea. Rev.*, **113**, 909–930, https://doi.org/10.1175/1520-0493(1985)113<0909:EOTSOP>2.0.CO;2.

Nakanish, M., 2001: Improvement of the Mellor–Yamada turbulence closure model based on large-eddy simulation data. *Bound.-Layer Meteor.*, **99**, 349–378, https://doi.org/10.1023/A:1018915827400.

Nieuwstadt, F. T. M., 1984: The turbulent structure of the stable, nocturnal boundary layer. *J. Atmos. Sci.*, **41**, 2202–2216, https://doi.org/10.1175/1520-0469(1984)041<2202:TTSOTS>2.0.CO;2.

Nolan, D. S., J. A. Zhang, and D. P. Stern, 2009a: Evaluation of planetary boundary layer parameterizations in tropical cyclones by comparison of in situ observations and high-resolution simulations of Hurricane Isabel (2003). Part I: Initialization, maximum winds, and the outer-core boundary layer. *Mon. Wea. Rev.*, **137**, 3651–3674, https://doi.org/10.1175/2009MWR2785.1.

——, D. P. Stern, and J. A. Zhang, 2009b: Evaluation of planetary boundary layer parameterizations in tropical cyclones by comparison of in situ observations and high-resolution simulations of Hurricane Isabel (2003). Part II: Inner-core boundary layer and eyewall structure. *Mon. Wea. Rev.*, **137**, 3675–3698, https://doi.org/10.1175/2009MWR2786.1.

Prandtl, L., 1925: 7. Bericht über untersuchungen zur ausgebildeten turbulenz. *Z. Angew. Math. Mech.*, **5**, 136–139, https://doi.org/10.1002/zamm.19250050212.

Rodier, Q., V. Masson, F. Couvreux, and A. Paci, 2017: Evaluation of a buoyancy and shear based mixing length for a turbulence scheme. *Front. Earth Sci.*, **5**, 65, https://doi.org/10.3389/feart.2017.00065.

Siebesma, A. P., P. M. M. Soares, and J. Teixeira, 2007: A combined eddy-diffusivity mass-flux approach for the convective boundary layer. *J. Atmos. Sci.*, **64**, 1230–1248, https://doi.org/10.1175/JAS3888.1.

Smith, R. K., and G. L. Thomsen, 2010: Dependence of tropical-cyclone intensification on the boundary-layer representation in a numerical model. *Quart. J. Roy. Meteor. Soc.*, **136**, 1671–1685, https://doi.org/10.1002/qj.687.

Stull, R. B., 1988: *An Introduction to Boundary Layer Meteorology*. Kluwer Academic Publishers, 670 pp.

Troen, I. B., and L. Mahrt, 1986: A simple model of the atmospheric boundary layer; sensitivity to surface evaporation. *Bound.-Layer Meteor.*, **37**, 129–148, https://doi.org/10.1007/BF00122760.

Vogelezang, D. H. P., and A. A. M. Holtslag, 1996: Evaluation and model impacts of alternative boundary-layer height formulations. *Bound.-Layer Meteor.*, **81**, 245–269, https://doi.org/10.1007/BF02430331.

Zhang, F., and Z. Pu, 2017: Effects of vertical eddy diffusivity parameterization on the evolution of landfalling hurricanes. *J. Atmos. Sci.*, **74**, 1879–1905, https://doi.org/10.1175/JAS-D-16-0214.1.

Zhang, J. A., and W. M. Drennan, 2012: An observational study of vertical eddy diffusivity in the hurricane boundary layer. *J. Atmos. Sci.*, **69**, 3223–3236, https://doi.org/10.1175/JAS-D-11-0348.1.

——, and E. W. Uhlhorn, 2012: Hurricane sea surface inflow angle and an observation-based parametric model. *Mon. Wea. Rev.*, **140**, 3587–3605, https://doi.org/10.1175/MWR-D-11-00339.1.

——, R. F. Rogers, D. S. Nolan, and F. D. Marks, 2011: On the characteristic height scales of the hurricane boundary layer. *Mon. Wea. Rev.*, **139**, 2523–2535, https://doi.org/10.1175/MWR-D-10-05017.1.

——, D. S. Nolan, R. F. Rogers, and V. Tallapragada, 2015: Evaluating the impact of improvements in the boundary layer parameterization on hurricane intensity and structure forecasts in HWRF. *Mon. Wea. Rev.*, **143**, 3136–3155, https://doi.org/10.1175/MWR-D-14-00339.1.